Theoretical and experimental study of the vibrational excitations in ethane monolayers adsorbed on graphite (0001) surfaces

F. Y. Hansen
Fysisk-Kemisk Institut, DTH 206, The Technical University of Denmark, DK-2800 Lyngby, Denmark
H. Taub
Department of Physics and Astronomy, University of Missouri-Columbia, Columbia, Missouri 65211

(Received 21 January 1987; accepted 24 April 1987)

The collective vibrational excitations of two different crystalline monolayer phases of ethane (C_2H_6) adsorbed on the graphite (0001) surface have been investigated theoretically and experimentally. The monolayer phases studied are the commensurate $\sqrt{3}\times 4$ structure in which the ethane molecules lie on their side in a herringbone arrangement and the commensurate $\sqrt{3}\times\sqrt{3}$ structure in which the molecules stand on-end with the C–C bond perpendicular to the surface. Semiempirical atom–atom potentials have been used to model the intermolecular and molecule–substrate interactions in calculations of the monolayer structure and lattice dynamics. The observed inelastic neutron scattering spectra below 4.1 THz are compared with calculated one-phonon incoherent cross sections. The calculated cross sections qualitatively reproduce the rather different spectra of the two phases and enable an identification of the observed vibrational modes. Moreover, they suggest that an important feature of the herringbone phase dynamics is a coupling of the lowest-frequency librational mode to the vibratory mode perpendicular to the surface. Calculations of the phonon dispersion relations, the phonon density of states, and the phonon contribution to heat capacities of the two monolayer phases are also presented and discussed.

I. INTRODUCTION

Over the past decade, inelastic neutron scattering (INS) has developed as one of the few techniques available for investigating the low-frequency ($\leqslant$25 THz) collective excitations of adsorbed monolayers.[1] Due to the weak neutron–film interaction, INS does not have the surface sensitivity of electron and neutral atom probes. Nevertheless, it has been used effectively to study the dynamics of strongly scattering monolayers adsorbed on high-surface-area substrates. The main experimental advantage which INS has over inelastic electron and He atom scattering is that ultrahigh vacuum is not required. On the theoretical side, the relative ease of calculating neutron–phonon cross sections enables a more quantitative comparison between observed and theoretical spectra than is possible with these other techniques.

Recent improvements in energy resolution have enabled measurements of the phonon dispersion relations of adsorbed monolayers on single crystal surfaces by inelastic electron[2] and He atom[3] scattering. While the use of polycrystalline substrates prevents such measurements by INS, there are several mitigating factors which should be considered. First, due to desorption effects, it is difficult to investigate the dynamics of physisorbed films by electron scattering. Second, in the case of He atom scattering, it has proved difficult to couple to vibrational modes involving atomic displacements parallel to the surface. Gibson and Sibener,[3] for example, only observed the dispersionless out-of-plane mode of a Kr monolayer on the Ag(111) surface. Excitation of the parallel modes is not prohibited by selection rules. Rather it requires directing the beam onto the sample at a small incident angle which is difficult to achieve experimentally. In contrast, it is relatively straightforward to observe by INS the translational modes of an adsorbate parallel as well as perpendicular to the substrate. The INS spectra are dominated by modes at the Brillouin zone boundaries where the phonon density of states is highest. In the one-phonon approximation, the mode intensities are proportional to the square of the phonon eigenvector projected on the neutron momentum transfer **Q**. Hence the observed intensity of the zone boundary modes depends sensitively on interactions within the film as well as the film–substrate coupling.

The capabilities of INS for investigating the collective excitations of adsorbed monolayers were first demonstrated in the case of the strongest coherent neutron scatterer, Ar^{36}, adsorbed on an exfoliated graphite substrate.[4] In these experiments, energy-loss peaks were observed corresponding to the zone-boundary longitudinal and transverse acoustic phonons polarized parallel to the surface as well as the out-of-plane mode of the monolayer. The mode intensities were found to be in reasonable agreement with model calculations of the one-phonon cross sections for a polycrystalline monolayer.

Due to the large incoherent cross section of hydrogen, hydrocarbons provide a large class of adsorbates whose dynamics can be studied by INS.[1] Moreover, they offer the opportunity to observe molecular librational modes absent in rare gas monolayers. Evidence of librational modes has been found in butane[1,5] and ethylene[6] films adsorbed on graphitized carbon substrates. However, these studies were hampered in the analysis of the INS spectra by uncertainty

 0021-9606/87/173232-14$02.10

in the monolayer structure, particularly the molecular orientations.

The dynamics of physisorbed hydrocarbons has also been investigated by inelastic He atom scattering. Mason and Williams[7] observed changes in the He energy-loss features of C_2H_6 (ethane) on the Ag (110) surface as the coverage was increased up to three layers. As in the case of the INS experiments on hydrocarbon monolayers, a detailed interpretation of the inelastic spectra was difficult without structural information.

Recently, two monolayer structures of ethane (C_2H_6) on the graphite (0001) surface have been solved by a combination of elastic neutron diffraction[8] and low-energy electron diffraction (LEED)[9] techniques. The low-density S1 phase has a commensurate structure in which the two molecules in the unit cell lie on their side in a herringbone pattern. It is similar to other herringbone structures which have been found for monolayers of N_2O_2,[10] N_2,[11] $Fe(CO)_5$,[12] and C_6H_{14} (hexane)[13] physisorbed on graphite. The high-density S3 phase has a $\sqrt{3}\times\sqrt{3}$ commensurate structure in which the single molecule per cell stands on its methyl tripod. The same structure has been inferred for submonolayer methane on the graphite (0001) surface.[14] Thus both ethane phases provide prototypical monolayer structures whose collective excitations can be investigated by INS. Another advantage of the C_2H_6/graphite system is that reliable empirical atom–atom potentials are available for calculation of the monolayer structure and lattice dynamics.

We have given a brief comparison of observed and calculated INS spectra for the two ethane monolayer phases on graphite in an earlier report.[15] Our purpose here is to give a more detailed account of this work. In Sec. II the semiempirical potentials are described followed by a discussion of the methods used to calculate the monolayer structure and lattice dynamics. Calculations of the phonon dispersion relations, the phonon density of states, the phonon contribution to the heat capacities, and the INS spectra are presented and discussed. In Sec. III, the theoretical and observed neutron–phonon cross sections are compared. The results are summarized in Sec. IV.

II. THEORY

A. Semiempirical potentials

Calculation of the structure and dynamics of the ethane monolayer phases adsorbed on graphite requires a knowledge of the intermolecular and molecule–substrate interactions. These interactions are of the weak van der Waals type in which no chemical bond is formed. Since a direct quantum mechanical calculation of them is prohibitively difficult even for a relatively small hydrocarbon molecule like ethane, we have modeled these interactions using semiempirical atom–atom potentials.[16] The method assumes that the intermolecular and molecule–substrate interactions can be expressed as a sum of potentials between atom pairs consisting of one atom from each interacting molecule or of an ethane and graphite atom, respectively. Furthermore, the atom–atom potentials are assumed to be derivable from central forces which depend only on the atom type and are independent of their chemical environment.

Various analytical expressions have been adopted to represent the atom–atom potential. The most common ones are included in the following expression:

$$\phi(r)=\frac{\epsilon(n+\lambda)}{(n+\lambda)-6}\cdot\left\{-\left(\frac{r_0}{r}\right)^6+\frac{6}{n+\lambda}\left(\frac{r_0}{r}\right)^n\exp\left[\lambda\left(1-\frac{r}{r_0}\right)\right]\right\}. \tag{1}$$

The four parameters ϵ, r_0, n, and λ can be given a direct physical interpretation. It is easy to see that ϵ is the depth of the potential well and r_0 is the equilibrium distance. The attractive part of the potential in Eq. (1) varies with distance as r^{-6} whereas different models of the repulsive part are obtained depending on the choice of n and λ. If $\lambda=0$, the repulsive part has an r^{-n} dependence as in the Lennard-Jones potential ($n=12$); if $\lambda\neq 0$ and $n\neq 0$, the repulsive part is a product of power law and exponential terms. Quantum calculations[17] support an exponential rather than a power law dependence of the repulsive part of the energy. In this case, $n=0$ in Eq. (1); and we obtain the Buckingham (6-exp) potential which can be written in the form

$$\phi(r)=-Ar^{-6}+B\exp(-\alpha r). \tag{2}$$

Upon comparing Eqs. (1) and (2), it is seen that

$$A=\frac{\epsilon\lambda r_0^6}{\lambda-6},\quad B=\frac{6\epsilon}{\lambda-6}\exp(\lambda),\quad \alpha=\frac{\lambda}{r_0}. \tag{3}$$

Unlike the parameters in Eq. (1), A, B, and α in Eq. (2) have no direct physical interpretation. They are determined by fitting experimentally observable properties of a series of compounds to those calculated from potentials of the form in Eq. (2). Such properties include crystal structure, heat of sublimation, elastic constants, and vibrational frequencies.

Considerable effort has been invested in determining pairwise-atomic potential parameters for the C–C, C–H, and H–H interactions of hydrocarbons. As discussed in Ref. 16, various criteria can be used to select among the different parameter sets available. One of the most important of these is the transferability of the potential parameters to other systems than those used in their determination. This is usually achieved by using a large number of different compounds in the parameter determination.[17,18] In the calculations described below, we have used the parameter sets of Kitaigorodskii[19] listed in Table I. Previous calculations found these to reproduce the lattice constants of a butane monolayer adsorbed on graphite better than several others tried.[1,20,21] The Kitaigorodskii potentials do not include the effects of electrostatic interactions caused by the intramolecular

TABLE I. Atom–atom potential parameters of Kitaigorodskii (Ref. 19). Parameters are defined in Eq. (2).

Atom pair	A (kcal Å^6/mol)	B (kcal/mol)	α (Å^{-1})	λ	r_0 (Å)	ϵ (kcal/mol)
C–C	359.0	42 040	3.58	13.58	3.79	0.0676
C–H	154.0	42 040	4.12	13.59	3.30	0.0666
H–H	57.6	42 040	4.86	13.57	2.79	0.0678

charge distribution.[22] We have recently begun to investigate their effect on the ethane monolayer structure[23]; but at this point, we do not believe that they would qualitatively alter the calculations of the monolayer lattice dynamics described below.

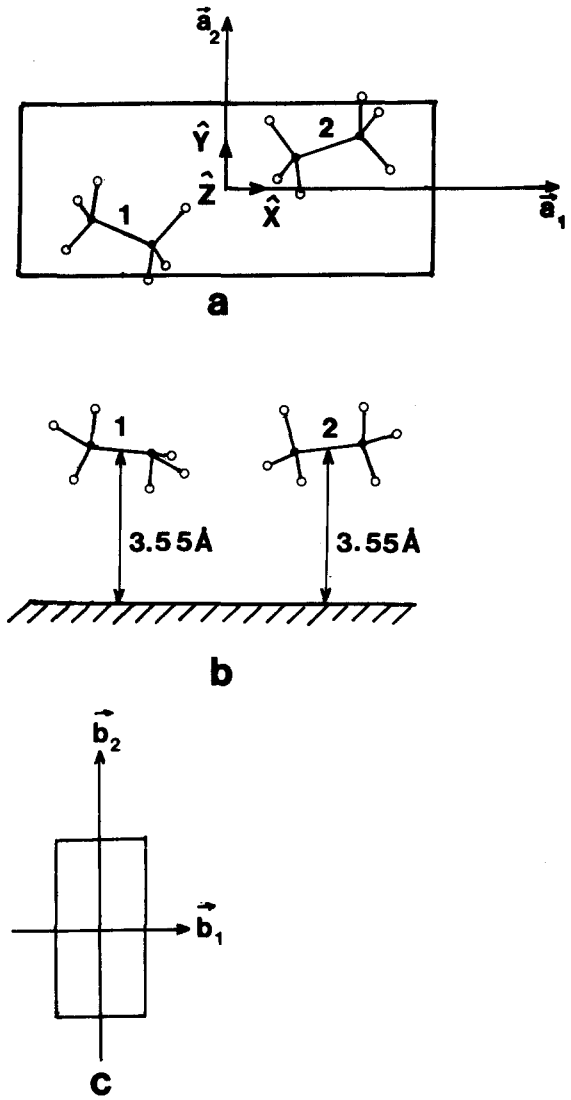

FIG. 1. The low-density structure S1 of monolayer ethane on the graphite (0001) surface: (a) projection on the graphite surface [cf. Fig. 1(a) in Ref. 15]; (b) side view; (c) reciprocal lattice vectors and first Brillouin zone; and (d) the lattice vectors $\mathbf{a}_i$ and reciprocal lattice vectors $\mathbf{b}_i$ of the S1 phase drawn in a coordinate system fixed to the graphite surface. The unit vector $\hat{z}$ is perpendicular to the surface.

B. The S1 and S3 monolayer phases of ethane on graphite and comparison with calculated structures

Ethane forms a variety of solid and liquid monolayer phases on the graphite (0001) surface as discussed in Refs. 8 and 9. In this paper, we restrict our attention to two commensurate solid phases which occur at low temperature. These are the lowest-density structure, S1, in which the molecules lie on their side with the C–C bond nearly parallel to the surface and the high-density structure, S3, in which they stand on end with the C–C bond perpendicular to the surface.[24]

The S1 phase has been observed at coverages from 0.4 to 0.8 layers and at temperatures below 60 K. Its LEED pattern[9] can be indexed with a rectangular unit cell of dimensions $(\sqrt{3}\times 4)a$, where a is the lattice constant of the graphite basal plane. The absence of reflections $(h,0)$ and $(0,k)$ with h and k odd is consistent with the herringbone structure with two molecules per unit cell shown in Fig. 1. The structure of the S1 phase has also been studied in neutron diffraction experiments with a deuterated film (C_2D_6) adsorbed on an exfoliated graphite substrate.[8] The Bragg peak positions in the neutron diffraction patterns are consistent with the commensurate $\sqrt{3}\times 4$ unit cell. In addition, it is possible to determine the molecular orientations by a kinematical analysis of the relative Bragg peak intensities in the neutron diffraction pattern.[8] Table II lists the experimentally inferred lattice constants and orientational parameters. The orientational parameters are defined in Fig. 2.

The high-density S3 phase is found at coverages $\geqslant 1.5$ layers and temperatures $\leqslant 80$ K. Both neutron diffraction[8] and LEED[9] experiments indicate a commensurate $\sqrt{3}\times\sqrt{3}$ structure on the graphite basal plane. Not enough Bragg peaks are observed in the neutron patterns to be able to determine the molecular orientations. However, simple packing arguments suggest the molecules are standing on end.

We have calculated the potential energy of monolayer clusters having the S1 and S3 ethane structure using the Buckingham potentials of Eq. (2) with the Kitaigorodskii parameters of Table I. The molecules were assumed to be rigid and in the staggered configuration. The (0001) graphite surface was simulated by a single honeycomb layer of

TABLE II. Comparison of the experimentally determined and calculated lattice constants and molecular orientational parameters for the S1 and S3 monolayer phases of ethane on graphite. All angles are given in degrees. θ is the angle between the lattice vectors $\mathbf{a}_1$ and $\mathbf{a}_2$.

Phase	a_1 (Å)	a_2 (Å)	θ	(α_1,α_2)[a]	(β_1,β_2)[a]	(ψ_1,ψ_2)[a]
S1						
Expt.[b]	9.87	4.26	90	(40,20)	(−10,−10)	(−67,−113)
Calc.	9.60	3.95	90	(45,15)	(−8,−8)	(−66,−112)
S3						
Expt.[b]	4.26	4.26	120	90[c]	90[c]	0[c]
Calc.	4.05	4.05	120	90	90	0

[a] Subscript refers to molecule identification number in Fig. 1(a).
[b] Reference 8.
[c] Assumed values. These parameters were not varied in the profile analysis of the neutron diffraction pattern.

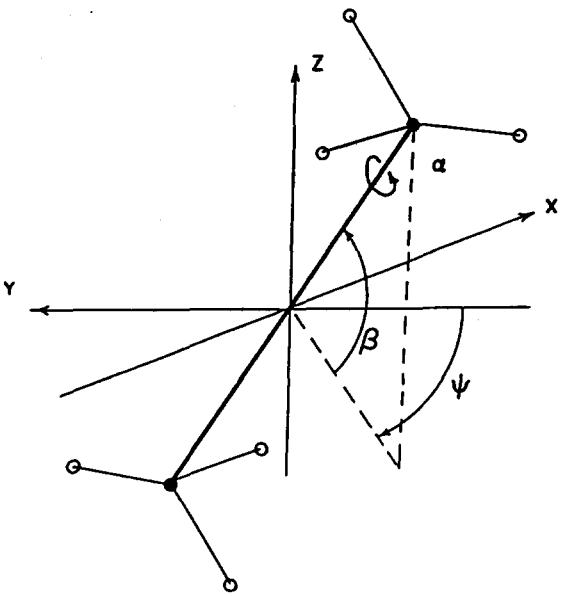

FIG. 2. The orientational parameters of the ethane molecule defined with respect to the Cartesian coordinate system in Fig. 1(d): α (rotation about the C–C axis), β (tilt of the C–C bond above the surface), and ψ (azimuthal orientation of the projection of the C–C bond on the surface). The zero of α corresponds to the configuration in Fig. 4 of Ref. 30. The C–C and C–H bond lengths are 1.53 and 1.09 Å, respectively.

carbon atoms, since deeper layers are beyond the cutoff lengths of the potentials.[25]

The potential energy minimization proceeded as follows. First the intermolecular energy of a cluster was minimized for a fixed location of the cluster on the graphite surface. Then the rigid cluster[26] was systematically translated in all three spatial directions and rotated about the surface normal to find the lowest cluster–substrate energy. At this location, the intermolecular cluster energy was optimized again; however, to the accuracy of our computations, it did not change from its original value. Repeating this process with the cluster initially at different sites on the graphite surface yielded the same results.

For the S1 structure, a cluster with three cells on a side (18 molecules) was used. The unit cell was constrained to be rectangular and the lattice constants and orientational parameters of both molecules systematically varied. The centers of mass of molecule nos. 1 and 2 were held fixed at positions $(-a_1/4, -a_2/4)$ and $(a_1/4, a_2/4)$, respectively, as in Fig. 1(a). The minimum energy of the cluster corresponded to the herringbone arrangement of the molecules in Fig. 1(a) with their center of mass at a height of 3.55 Å above the layer of graphite carbon atoms [Fig. 1(b)]. The orientational parameters α and β are such as to allow three H atoms in each molecule to be nearly in the same plane parallel to the surface. The calculated lattice constants and orientational parameters are listed in Table II. In the minimum energy configuration of the S1 cluster, the intermolecular energy is calculated to be -3.25 kcal/molecule and the molecule–substrate energy is -4.98 kcal/molecule.

In the case of the S3 structure, a hexagonal cluster containing seven molecules (one per unit cell) was used as shown in Fig. 3(a). In the minimization of the intermolecular potential, the unit cell was assumed to be hexagonal and the molecules to be oriented with the C–C bond perpendicular to the surface. Only the lattice constant and the molecular angle of rotation (ψ) about the surface normal were varied. The minimum in the intermolecular energy occurs for the nested arrangement of the methyl tripods shown in Fig. 3(a) in which an H atom from one molecule lies in the cleavage between two H atoms in a neighboring molecule. For this S3 cluster, we find an intermolecular energy of -4.17 kcal per molecule and a molecule–substrate energy of -4.16 kcal/molecule. The height of the molecular center of mass was found to be 4.01 Å as shown in Fig. 3(b).

Table II shows that the calculated and observed molecular orientations for the S1 structure agree within the experimental uncertainty of $\pm 10°$. Generally, the calculated lattice constants are smaller than observed so that neither the S1 nor the S3 phase are predicted to be commensurate with the graphite basal plane. This discrepancy between the calculated and observed lattice constants is as large as 7%. We believe that the computed structures are sufficiently accurate to justify calculations of the lattice dynamics of both phases with the Kitaigorodskii potentials.

C. Description of the monolayer lattice dynamics calculations

1. Coordinate selection

In the conventional theory of lattice dynamics developed by Born and Huang,[27] the potential energy of a crystal is expanded in powers of the Cartesian displacements of the constituent atoms. The harmonic approximation is made in the expansion about the potential minimum so that cubic and higher order terms in the displacements are neglected. The use of Cartesian displacements is not well adapted to molecular crystals, since one cannot exploit the division of force constants into relatively large values for intramolecular coordinates and smaller ones for intermolecular interactions. In the case of the ethane/graphite system, we use an extreme limit of the molecular crystal approach in which the ethane molecule is assumed rigid except for the torsion of the methyl groups about the C–C bond. The methyl torsion is the lowest frequency internal mode and the only one to be measurably perturbed by adsorption. INS spectra show a shift of the methyl torsion frequency from 8.7 THz for the free molecule[28] to 9.1 THz for the S3 monolayer phase[29] in agreement with calculated estimates.[30] We shall see that the methyl torsion is the only intramolecular mode to couple significantly to lattice modes of the ethane monolayer.

Another approximation which we have made is to neglect any motion of the carbon atoms in the graphite substrate. Theoretical studies of the dynamics of xenon[31] and krypton[32] adsorbed on graphite have shown that resonance effects between monolayer and graphite modes become important only at low frequencies and wave vectors near the Brillouin zone center. Since our main interest is the calculation of neutron–phonon cross sections which are dominated by modes near the Brillouin zone boundary, we shall assume such resonance effects to be unimportant.

To express the intermolecular and molecule–substrate

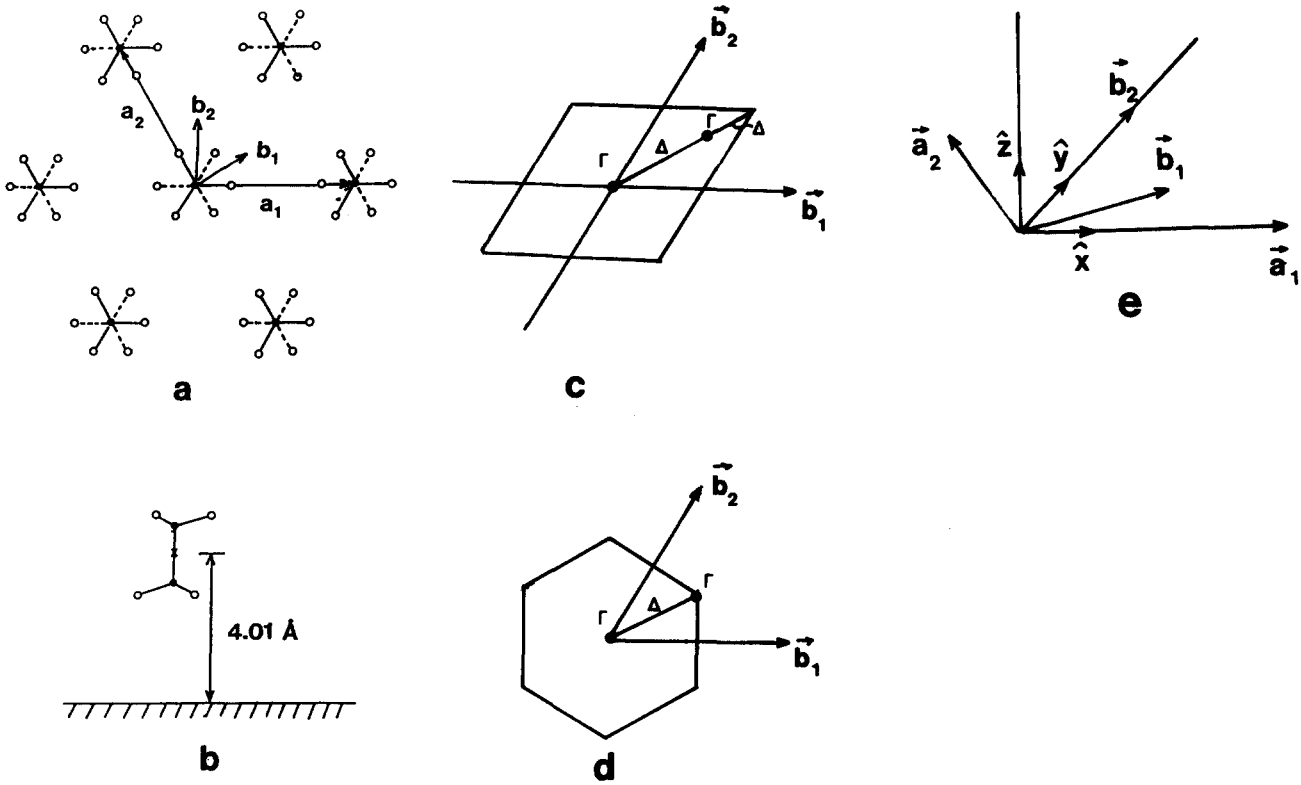

FIG. 3. The high-density structure S3 of monolayer ethane on the graphite (0001) surface: (a) projection on the graphite surface. The dashed lines represent C–H bonds of the methyl group closest to the surface; (b) side view; (c) reciprocal lattice vectors $\mathbf{b}_i$ and the oblique Brillouin zone; (d) the hexagonal Brillouin zone; and (e) the lattice vectors $\mathbf{a}_i$ of the S3 phase drawn in a coordinate system fixed to the surface [as in Fig. 1(d)]. The unit vector $\hat{z}$ is perpendicular to the surface.

parts of the potential energy function, we use a method developed previously for molecular crystals.[33] The force constants are defined in terms of relative translational and rotational coordinates. The excitation H_i of the ith coordinate is obtained by operating on the actual displacement of the atoms $\Delta\mathbf{R}$ with the projection operator $\mathbf{B}_i$:

$$H_i = \mathbf{B}_i \cdot \Delta\mathbf{R}, \tag{4}$$

where

$$\Delta\mathbf{R} = \begin{bmatrix} \Delta\mathbf{R}_1 \\ \Delta\mathbf{R}_\nu \\ \Delta\mathbf{R}_N \end{bmatrix}, \quad \Delta\mathbf{R}_\nu = \begin{bmatrix} \Delta x_\nu \\ \Delta y_\nu \\ \Delta z_\nu \end{bmatrix} \tag{5}$$

and

$$\mathbf{B}_i = [\mathbf{B}_{11},\ldots,\mathbf{B}_{i\nu},\ldots,\mathbf{B}_{iN}], \tag{6a}$$

$$\mathbf{B}_{i\nu} = [\mathbf{B}_{i\nu,x},\mathbf{B}_{i\nu,y},\mathbf{B}_{i\nu,z}]. \tag{6b}$$

N is the number of atoms in the monolayer. The potential energy function V is then expressed in terms of the coordinates H_i by

$$V = \tfrac{1}{2}\mathbf{H}^T\mathbf{F}\mathbf{H} = \tfrac{1}{2}\Delta\mathbf{R}^T[\mathbf{B}^T\mathbf{F}\mathbf{B}]\Delta\mathbf{R} \tag{7}$$

with

$$\mathbf{H} = \begin{bmatrix} H_1 \\ \vdots \\ H_j \\ \vdots \\ H_N \end{bmatrix} \text{ and } \mathbf{F} = \begin{bmatrix} F_{11} & \cdots & F_{1N} \\ \vdots & & \vdots \\ F_{N1} & \cdots & F_{NN} \end{bmatrix}, \tag{8}$$

where $\mathbf{F}$ is the force constant matrix.

The intermolecular potential energy function is expressed as a sum of molecule–pair interactions. Due to the short range of the van der Waals forces, it is only necessary to include nearest and, in the case of the S1 structure, next-nearest neighbor pairs. For a given pair of molecules, eight coordinates are considered as listed in Table III. They are defined with respect to a local coordinate system (x,y,z) with origin at the center of mass of one molecule in the pair and the x axis taken along the direction toward the center of

TABLE III. The eight displacement coordinates of a molecular pair (i,j) used to express the intermolecular potential energy function. Subscripts refer to the local coordinate system (x,y,z) defined in the text. θ_α is a rotation of a molecule about the α axis, and t_α is a translation of a molecule along the α axis. All of the coordinates are invariant to crystal translations. Those lacking invariance to crystal rotation are indicated in the last column.

Coordinate number	Molecule i	Molecule j	Invariant to crystal rotation?
1	θ_x	$-\theta_x$	yes
2	θ_y	$-\theta_y$	yes
3	θ_z	$-\theta_z$	yes
4	θ_y	θ_y	no
5	θ_z	θ_z	no
6	t_x	$-t_x$	yes
7	t_y	$-t_y$	no
8	t_z	$-t_z$	no

mass of the other molecule. It is straightforward to transform from this coordinate system to the one used in the lattice dynamics calculations [see Figs. 1(d) and Fig. 3(e)].

The coordinates listed in Table III are sufficient to describe the intermolecular interactions completely. Moreover, they are convenient to use since they satisfy most of the invariance requirements with respect to crystal translations and rotations. The rotational invariance lacking in coordinates 4, 5, 7, and 8 can be achieved by introducing the following off-diagonal terms in the force constant matrix:

$$F_{47} = -\tfrac{1}{2}[F_{44} + F_{77}],$$
$$F_{58} = -\tfrac{1}{2}[F_{55} + F_{88}] \quad (9)$$

and by proper definition of the projection operators $\mathbf{B}_l$ in Eq. (4).

For the molecule–substrate interaction, we use six coordinates corresponding to three rotations and three translations of a molecule about the axes of the coordinate system fixed to the substrate [Figs. 1(d) and 3(e)]. These coordinates are not orthogonal to translations and rotations of the monolayer due to the symmetry breaking of the graphite substrate.

As discussed above, the intramolecular potential contains only one coordinate corresponding to the methyl torsion about the C–C bond of the molecule.

We note that application of a symmetry operation of the monolayer to any one of the coordinates considered yields an equivalent coordinate having the same force constant. In the computer code which we have used, it is only necessary to define a set of independent basis coordinates which are unrelated by symmetry operations.[34] All equivalent coordinates are generated automatically and assigned the proper force constants.

For the S3 monolayer phase, only nearest-neighbor interactions were included in the intermolecular potential. The next-nearest neighbors in this high-symmetry phase (C_{3V}^2 space group[35]) are beyond the 10 Å cutoff assumed for the pairwise atomic potentials.[25] There are then a total of 15 basis coordinates: 8 for the intermolecular interaction, 6 for the molecule–substrate interaction, and 1 for the intramolecular methyl torsion.

Due to the lower symmetry of the S1 phase, a much larger set of basis coordinates is required. Next-nearest neighbors are within the cutoff range of the intermolecular potential so that six different molecular–pair interactions must be included as illustrated in Fig. 4. The following interactions of molecule 2 in the unit cell (0,0) are considered: (a) with molecule 2 in cell (0,1), (b) with molecule 1 in cell (0,1), (c) with molecule 1 in cell (1,1), (d) with molecule 1 in cell (1,0), (e) with molecule 1 in cell (0,1), and (f) with molecule 1 in cell (0,0). The interactions between molecule 1 in cell (0,0) and those in neighboring cells are equivalent to those enumerated above and are not included in the basis set. Interactions (a) and (e) are between nearest neighbors (intermolecular distance of 3.90 Å) and (b), (c), and (d) are between next-nearest neighbors (intermolecular distance of 5.18 Å). Since eight coordinates are required (see Table III) to describe each of the molecular–pair interactions in Fig. 4, we have $6 \times 8 = 48$ nonequivalent intermolecular coordinates. The interaction of each molecule with the substrate is described by the same six coordinates used for the S3 phase. This gives $2 \times 6 = 12$ additional basis coordinates. Including the methyl torsion of each molecule, yields a total of 62 basis coordinates for the S1 monolayer phase.

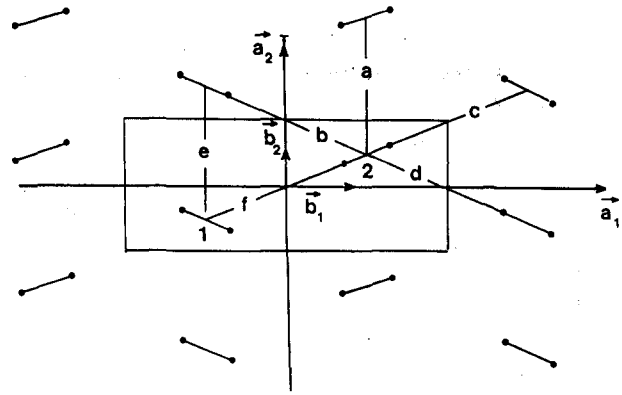

FIG. 4. Diagram illustrating the molecular pair interactions in the S1 monolayer ethane phase. Pairs (a) and (e) are nearest neighbors (3.90 Å separation); (b), (c), and (d) are next-nearest neighbors (5.18 Å separation); and (f) is the pair within the unit cell (5.18 Å separation).

2. Evaluation of force constants

The semiempirical atom–atom potentials described in Sec. II A have been used to calculate the force constants defined in Eqs. (7) and (8). To obtain the intermolecular interaction, the potential energy of a pair of molecules is calculated as a function of one of the eight basis coordinates described above. For the molecule–substrate interaction, the potential energy of a single molecule interacting with the layer of graphite carbon atoms is calculated as a function of one of the six rotational and translational coordinates. In each case, the force constant is taken to be the second derivative of the potential energy function of the appropriate coordinate evaluated at its equilibrium value. A similar method is used to determine the intramolecular methyl torsion force constant except that the potential barrier used is that calculated quantum mechanically for a free molecule.[36]

In general, the number of distinct elements in the symmetric force constant matrix [Eq. (8)] can be as large as 120 for the S3 structure and 1953 for the S1 phase. In order to simplify the calculation for the S3 phase, we have assumed all off-diagonal elements of the force constant matrix to be zero except those required by Eqs. (9) for rotational invariance and those involving the coupling of the methyl torsion to the θ_z molecular rotation as described below.[37] We shall see that this force constant matrix allows us to reproduce the qualitative features of the INS spectrum for the S3 phase. In the case of the S1 phase, we have been able to reproduce the INS spectra reasonably well by including only one other off-diagonal element in the force constant matrix besides those required by Eqs. (9) and the coupling of the methyl torsion to lattice modes. We shall describe in the next section how both the observed spectra and symmetry considerations led us to consider this additional coupling constant.

D. Results

1. Phonon dispersion relations, density of states, and heat capacity

a. S3 phase. In Figs. 3(c) and 3(d) are shown two choices of the Brillouin zone for the hexagonal S3 phase. For our lattice dynamics calculations, we have selected the oblique zone in Fig. 3(c) spanned by the reciprocal lattice vectors $\mathbf{b}_1$ and $\mathbf{b}_2$. In Fig. 3(e) they are drawn along with the direct lattice vectors $\mathbf{a}_1$ and $\mathbf{a}_2$ in the Cartesian coordinate system used in our calculations (note that $\hat{z}$ is perpendicular to the surface).

The calculated phonon dispersion relations for the S3 monolayer phase are shown in Fig. 5 for wave vectors in the directions of $\mathbf{b}_1$ (or $\mathbf{b}_2$) and $\mathbf{b}_1 + \mathbf{b}_2$. The branches are labeled with the symmetry symbols shown in Fig. 3(c). At the zone center there are two one-dimensional irreducible representations Γ_1 and Γ_2 and one two-dimensional irreducible representation Γ_3. Along the direction of $\mathbf{b}_1$ (or $\mathbf{b}_2$) there is only translational symmetry. In the $\mathbf{b}_1 + \mathbf{b}_2$ direction the symmetry is described by two one-dimensional irreducible representations Δ_1 and Δ_2. At the wave vector $1/3(\mathbf{b}_1 + \mathbf{b}_2)$ corresponding to the zone boundary of the hexagonal Brillouin zone [Fig. 3(d)], the symmetry is the same as at Γ. Consequently, there should be two doubly degenerate modes as verified by the calculations.

The highest branch in the dispersion curves of Fig. 5 is the methyl torsional mode. We have considered the coupling between the methyl torsion coordinate and the other basis coordinates of the S3 phase as follows. At Γ, the only lattice mode with the same symmetry (Γ_2) as the methyl torsion and hence the only mode to which it can couple is the one involving the θ_z rotation of the molecule about the C–C bond (z axis). The situation changes along Δ where, in addition to the θ_z rotation, the rotation about the y axis θ_y and the translations in the x and y directions t_x and t_y also have the same symmetry as the methyl torsion. However, our calculations have shown that couplings to these other modes produce no effect on the methyl torsion.

The θ_z rotation of the molecule occurs in 3 of the 15 basis coordinates. One of these is the rotation of a single molecule with respect to the surface. Due to the small corrugation of the molecule–substrate potential, the restoring force associated with this coordinate is so weak that we can neglect its coupling to the methyl torsion. The other two basis coordinates which involve the θ_z rotation are those in which a nearest-neighbor pair of molecules rotate in either the same or opposite sense (types 3 and 5 in Table III). Only rotation in the same direction will be excited at the zone center while only opposite-sense rotation will be excited at the zone boundary. Since the density of states is highest at the zone boundary, the opposite-sense rotations will contribute more strongly to the INS spectrum. Therefore, we have only included a coupling of the methyl torsion to this basis coordinate. As can be seen in Fig. 5, it results in a slight dispersion of the methyl torsion branch from the free-molecule value of 8.7 THz at Γ to 9.1 THz at the zone boundaries.

The θ_z rotational mode lies just below the methyl torsion branch at the Γ point where it has a frequency of $\sim$7.5 THz. This mode is strongly dispersed, dropping to $\sim$4.4 THz at the zone boundary. Coupling to the methyl torsional mode introduces a small admixture of torsional motion into its eigenvector.

We continue by briefly describing the other phonon branches in the dispersion curves of Fig. 5. The two Γ_3 modes with frequencies of $\sim$4.1 THz at the zone center involve rocking motions θ_x and θ_y of the molecules about the x and y axes, respectively. They are not dispersed as strongly as the higher-frequency θ_z mode due to the larger restoring force for molecular rotations about the x and y axes parallel

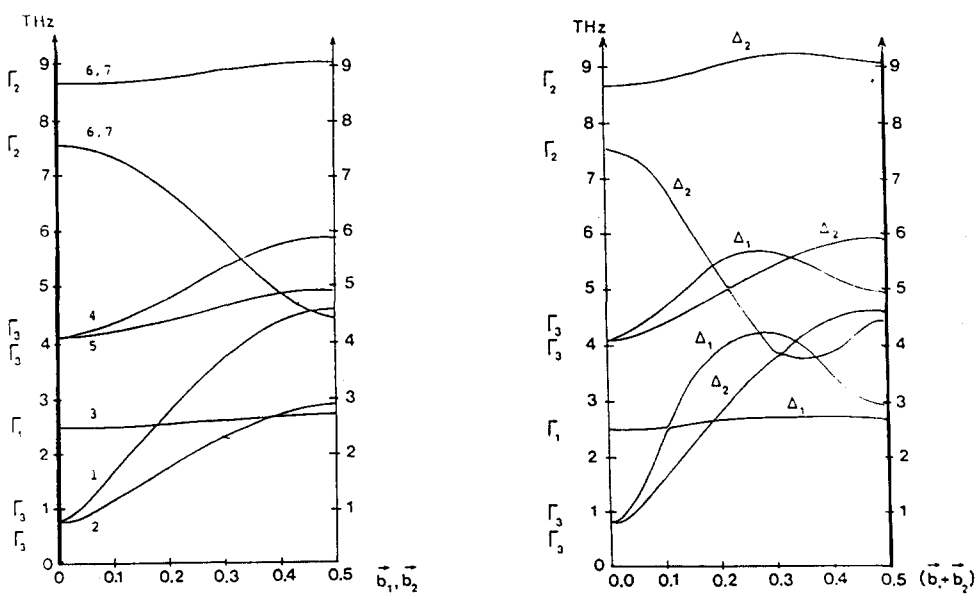

1	2	3	4	5	6	7
t_x, t_y	t_x, t_y	t_z	θ_x, θ_y	θ_x, θ_y	θ_z	H_3C-CH_3

FIG. 5. Phonon dispersion relations calculated for the S3 phase. The branches are identified by their point-group symmetry label defined in Fig. 3(c) and also by numbers in the left panel appearing in the table at the bottom of the figure. This table lists the types of molecular motion using the same translation and rotation symbols as in Table III. Note that the subscripts now refer to the coordinate system fixed in the substrate as in Fig. 3(e).

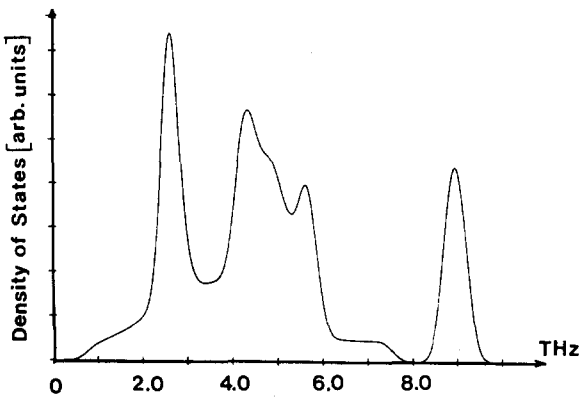

FIG. 6. Phonon density of states calculated for the S3 phase after folding with a Gaussian resolution function (FWHM = 1.8 THz).

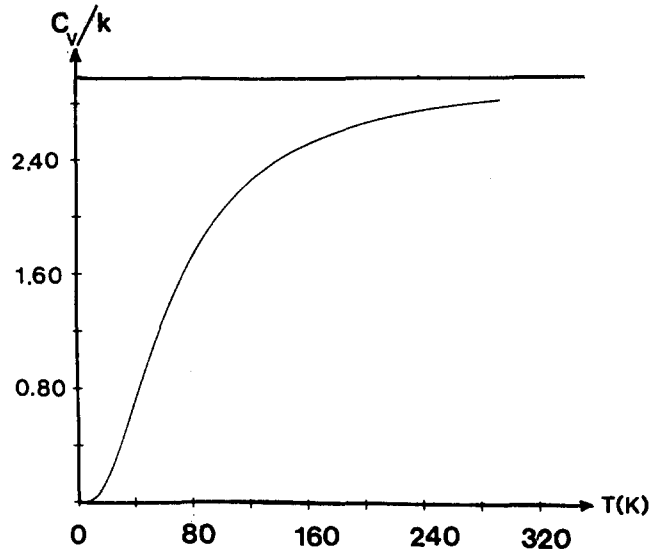

FIG. 7. Temperature dependence of the phonon contribution to the monolayer heat capacity per molecule calculated for the S3 phase. The heat capacity is expressed in reduced units C_v/k_B where k_B is Boltzmann's constant. The S3 phase is believed to melt near 80 K (see Refs. 8 and 9).

to the surface. The Γ_1 mode with frequency of $\sim$2.5 THz corresponds to bouncing of the molecules against the surface. It is nearly dispersionless, since the restoring force is almost entirely determined by the molecule–substrate interaction. In this mode, the molecules behave nearly as independent oscillators.

The two lowest modes at the zone center involve translations of the molecules along the x and y axis parallel to the surface. They have Γ_3 symmetry at the zone center and are strongly dispersed. The nonzero frequency ($\sim$0.7 THz) at the Γ point is a result of the corrugation of the adatom–surface potential.

The phonon density of states calculated for the S3 phase is shown in Fig. 6. We found that a sampling of 800 points in half of the Brillouin zone was sufficient to achieve convergence. The large, narrow peaks correspond to the nearly dispersionless translational mode normal to the surface at $\sim$2.5 THz and the methyl torsional mode at $\sim$9.0 THz. The broader feature in the range 4 to 6 THz results from the flat regions of the more strongly dispersed branches. Finally, we have used the normalized density of states $g(\nu)$ to calculate C_v, the phonon contribution to the monolayer heat capacity per molecule, from the expression

$$\frac{C_v}{k_B} = \int_0^\infty \frac{(h\nu/k_BT)^2 \exp(-h\nu/k_BT)}{[1-\exp(-h\nu/k_BT)]^2} g(\nu)d\nu, \quad (10)$$

where ν is the phonon frequency, T is the temperature, h is Planck's constant, and k_B is Boltzmann's constant. The heat capacity of the S3 phase is plotted as a function of the temperature in Fig. 7. We find the zero point energy of the S3 phase to be 340 K per molecule.

b. S1 phase. The Brillouin zone for the rectangular S1 structure is shown in Fig. 1(c). The dispersion relations for wave vectors in the $\mathbf{b}_1$ and $\mathbf{b}_2$ directions appear in Fig. 8.

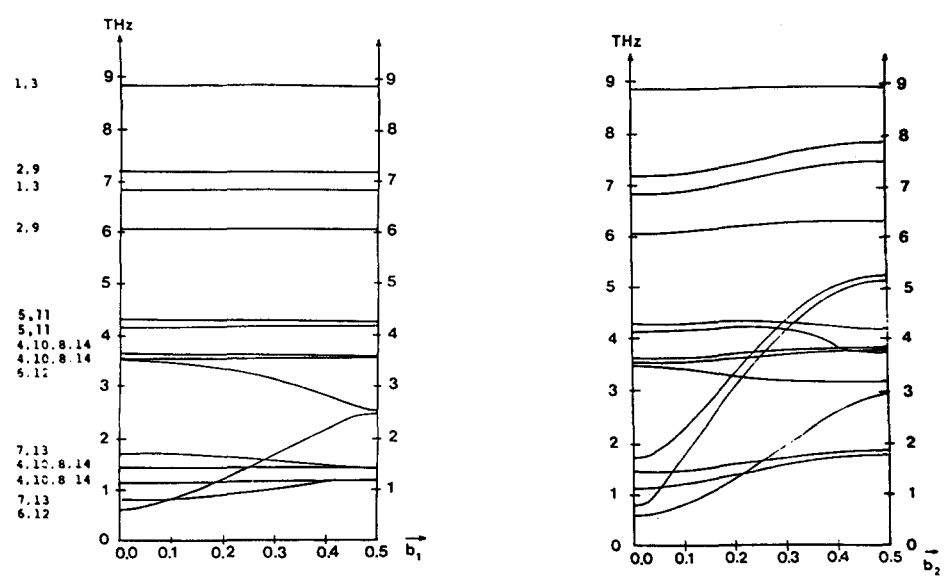

Molecule	2	3	4	5	6	7	8
1	H_3C-CH_3	θ_x	θ_y	θ_z	t_x	t_y	t_z

Molecule	1	9	10	11	12	13	14
2	H_3C-CH_3	θ_x	θ_y	θ_z	t_x	t_y	t_z

FIG. 8. Phonon dispersion relations calculated for the S1 phase. The numbers at left refer to the table at the bottom of the figure listing the types of motion for each molecule. The translation and rotation symbols are the same as in Table III except that the subscripts refer to the coordinate system fixed in the substrate shown in Fig. 1(d).

With two molecules per unit cell, there are a total of 14 branches, i.e., twice as many as for the S3 structure. Due to the low symmetry of the S1 phase, the character of the modes is rather complex and usually a mixture of several types of motion.

The highest frequency branch at ~ 8.7 THz involves methyl torsional motion predominantly. INS experiments[29] indicate a smaller perturbation of the methyl torsion than in the S3 phase. Since no symmetry arguments can be invoked to infer its coupling to other modes, we have assumed it to be coupled only to the molecular rotation about the C–C bond (θ_x) as in the S3 phase. The coupling constant was adjusted to give a dispersion in the methyl torsion frequency consistent with earlier experiments.[29]

The three branches with frequencies in the range 6–8 THz are modes in which there is a mixture of a θ_x rotation and methyl torsional motion. Because the C–C bond is nearly parallel to the surface in the S1 phase, the force constant for the θ_x rotation is determined primarily by the molecule–substrate interaction. This results in little dispersion of these branches.

The flat branches at ~ 4.25 and ~ 4.1 THz correspond to modes in which the two molecules in the unit cell rotate about the surface normal (θ_z rotations) in the same and the opposite sense, respectively. The lack of dispersion in these modes indicates that the main contribution to the restoring forces comes from the interaction between two molecules within a unit cell.

The molecular motions associated with the branches at 1.1, 1.4, 3.55, and 3.65 THz are combinations of rotations about the y axis (θ_y) and translations along the z axis (t_z). Like the θ_x rotational modes, these show little dispersion since the dominant restoring force arises from the molecule–substrate interaction.

All of the pure translational modes are strongly dispersed. This is particularly true for wave vectors along $\mathbf{b}_2$ which is the direction of the nearest-neighbor bonds labeled (a) and (e) in Fig. 4. The branches with frequencies of ~ 3.5 and ~ 1.7 THz at the zone center correspond to opposite translations of the two molecules in the unit cell along the x and y axis, respectively. They are analogous to the optical mode in a linear chain with two atoms per unit cell. The branches with the two lowest frequencies at the zone center involve translations of the two molecules in the unit cell in the same sense along the x and y axes. Note again the much larger dispersion along $\mathbf{b}_2$ for the t_y modes in which the molecules move parallel to their nearest-neighbor bonds.

The dispersion relations in Fig. 8 have been computed assuming an additional off-diagonal element in the force constant matrix which was not described in Sec. II C 2. This force constant couples translational motion of a molecule along the surface normal to rotational motion about an axis which is perpendicular to the C–C bond and parallel to the surface. The motivation for including this coupling will be discussed in Sec. III where the calculated and observed inelastic neutron cross sections are compared. For now, we simply note the effect of this coupling on the dispersion relations. Without the coupling, the two pairs of branches labeled 4, 10, 8, 14 collapse into a narrow band of modes in the range 2.5 to 3.0 THz as illustrated in Fig. 9.

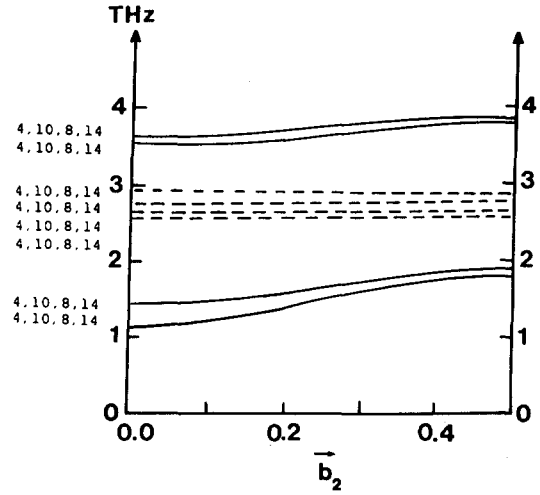

FIG. 9. Effect on the phonon dispersion curves of a coupling between the θ_y rotation and t_z translation coordinates (see Table III) in the S1 phase. The affected branches are shown without a coupling (dashed curves) and after introducing a coupling (solid lines).

The large number of phonon branches of the S1 phase is reflected in the complexity of the density of states shown in Fig. 10. The temperature dependence of the heat capacity of this phase calculated from Eq. (10) is plotted in Fig. 11. We find the zero point energy of the S1 phase to be 310 K per molecule.

2. Calculation of the inelastic neutron cross sections for the S1 and S3 phases

One of the principal advantages of neutron scattering over other probes of surface dynamics is the relative simplicity of calculating the neutron–phonon cross sections. In the case of hydrocarbon films the calculations are further simplified by the large incoherent cross section of hydrogen for thermal neutrons. Using the cross sections listed in Table IV,[38] we estimate the error in neglecting the coherent scattering from the C and H nuclei to be less than 3%.

The incoherent, one-phonon cross section for thermal neutrons of a lattice with n atoms per unit cell is given by[39]

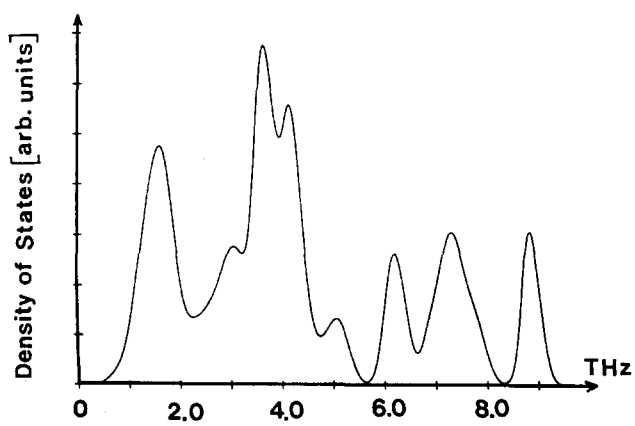

FIG. 10. Phonon density of states calculated for the S1 phase after folding with a Gaussian resolution function (FWHM = 1.8 THz).

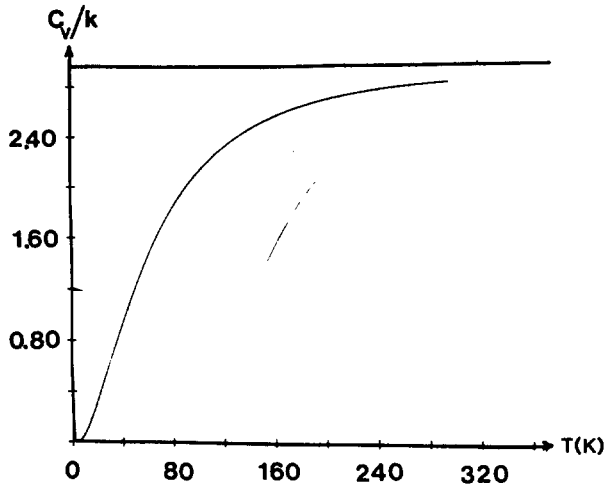

FIG. 11. Temperature dependence of the phonon contribution to the monolayer heat capacity per molecule calculated for the S1 phase. The heat capacity is expressed in reduced units C_v/k_B where k_B is Boltzmann's constant. Note that near 64 K the S1 phase undergoes a transition to an I1 phase in which the molecules are orientationally disordered. (See Refs. 8 and 9.)

$$\frac{d^2\sigma}{d\Omega dE} = \frac{1}{8\pi}\frac{k'}{k}\sum_{d=1}^{n}\sigma_{\mathrm{inc},d} \times e^{-2W_d(\mathbf{Q})}\frac{1}{M_d}\sum_{j,\mathbf{q}}\frac{1}{\omega_j(\mathbf{q})}|\mathbf{Q}\cdot\boldsymbol{\sigma}_d^j(\mathbf{q})|^2 \times\{[n_j(\mathbf{q})+1]\cdot\delta[\omega-\omega_j(\mathbf{q})] + n_j(\mathbf{q})\cdot\delta[\omega+\omega_j(\mathbf{q})]\}. \quad (11)$$

In this expression, k and k' are the magnitudes of the incident and scattered neutron wave vector, respectively; $\sigma_{\mathrm{inc},d}$ is the incoherent scattering cross section for atom d, $W_d(\mathbf{Q})$ its Debye–Waller factor, and M_d its mass. The phonon of the jth band at the reduced wave vector $\mathbf{q}$ has frequency $\omega_j(\mathbf{q})$ and eigenvector $\boldsymbol{\sigma}_d^j(\mathbf{q})$ with a population factor $n_j(\mathbf{q})$ given by

$$n_j(\mathbf{q}) = \frac{1}{\exp[\hbar\omega_j(\mathbf{q})/k_BT]-1}. \quad (12)$$

In Eq. (11), the factor $\delta[\omega+\omega_j(\mathbf{q})]$ corresponds to phonon annihilation (neutron energy gain) while $\delta[\omega-\omega_j(\mathbf{q})]$ represents phonon creation (neutron energy loss).

For both the S1 and S3 monolayer ethane phases, we have calculated the incoherent, one-phonon cross section of Eq. (11). As in the case of the phonon density of states, the summation over $\mathbf{q}$ was performed by sampling half of the Brillouin zone with a uniform mesh of 800 points. At each point, the frequencies $\omega_j(\mathbf{q})$ of all branches and their associated eigenvectors $\boldsymbol{\sigma}_d^j(\mathbf{q})$ were computed. The Debye–Waller factors for all of the atoms were set equal to zero. This assumption is believed to be reasonable for comparing the calculated cross section with the observed spectra taken at ~ 10 K.

TABLE IV. Thermal neutron cross sections of carbon and hydrogen in barns from Ref. 38.

Nucleus	σ_{total}	σ_{coh}	σ_{inc}
C	5.51	5.49	0.02
H	81.5	1.80	79.7

To obtain a sufficient intensity of inelastically scattered neutrons from the films, a large-surface-area, polycrystalline substrate must be used. In our experiments, the substrate was a recompressed exfoliated graphite known as Grafoil[40] which is rolled into thin sheets. Previous studies[4] have assumed a two-component model for the distribution of particle orientations in the graphite sheets: (1) an oriented component in which the c axes of the particles have a Gaussian distribution in angle about the sheet normal (full width at half-maximum $\sim 30°$); and (2) an isotropic component. The partial orientation of the substrate is of importance due to the factor $|\mathbf{Q}\cdot\boldsymbol{\sigma}_d^j(\mathbf{q})|^2$ in the cross section of Eq. (11). One expects a difference in the inelastic spectra depending on whether the wave vector $\mathbf{Q}$ is parallel or perpendicular to the Grafoil sheets. For example, vibrational modes which involve atomic displacements predominantly normal to the graphite basal plane surfaces should have their intensity enhanced in the $\mathbf{Q}$ perpendicular configuration.

In the case of an isotropic substrate, the factor $|\mathbf{Q}\cdot\boldsymbol{\sigma}_d^j(\mathbf{q})|^2$ in the one-phonon cross section can be replaced by its spherical average $\frac{1}{3}|\mathbf{Q}|^2|\boldsymbol{\sigma}_d^j(\mathbf{q})|^2$ so that for neutron-energy-loss scattering, Eq. (11) becomes

$$\frac{d^2\sigma}{d\Omega dE} = \frac{1}{24\pi}\frac{k'}{k}\sum_{d=1}^{n}\sigma_{\mathrm{inc},d} \times e^{-2W_d(\mathbf{Q})}\frac{1}{M_d}\sum_{j,\mathbf{q}}\frac{|\mathbf{Q}|^2|\boldsymbol{\sigma}_d^j(\mathbf{Q})|^2}{\omega_j(\mathbf{q})} \times[n_j(\mathbf{q})+1]\delta[\omega-\omega_j(\mathbf{q})]. \quad (13)$$

We have simulated the incoherent, one-phonon cross section of the S1 and S3 monolayer phases in both the $\mathbf{Q}$ perpendicular and parallel configurations for a purely Gaussian particle distribution. At each point in the Brillouin zone, the cross section in Eq. (11) is averaged over 100 different $\mathbf{Q}$ orientations conforming to the Gaussian distribution about the surface normal (perpendicular configuration) or the surface plane (parallel configuration). A sampling of 100 orientations was deemed sufficient since the results did not change significantly upon increasing the number from 70 to 100. In both the perpendicular and parallel configurations, the projection of $\mathbf{Q}$ on the surface is assumed to be directed randomly with respect to the monolayer lattice.

The effect of the particle orientation distribution function on the calculated cross sections is illustrated in Fig. 12 for the higher-symmetry S3 phase. One can see that, as expected, the translational mode normal to the surface at 2.5 THz is strongly enhanced in the $\mathbf{Q}$ perpendicular configuration [Fig. 12(a)] while in the parallel configuration [Fig. 12(b)] the intensity of the translational modes parallel to the surface increases in the frequency range from 4 to 6 THz.

III. COMPARISON OF THEORETICAL AND OBSERVED CROSS SECTIONS

The observed neutron-loss spectra were obtained with the Mitsubishi triple-axis spectrometer at the University of

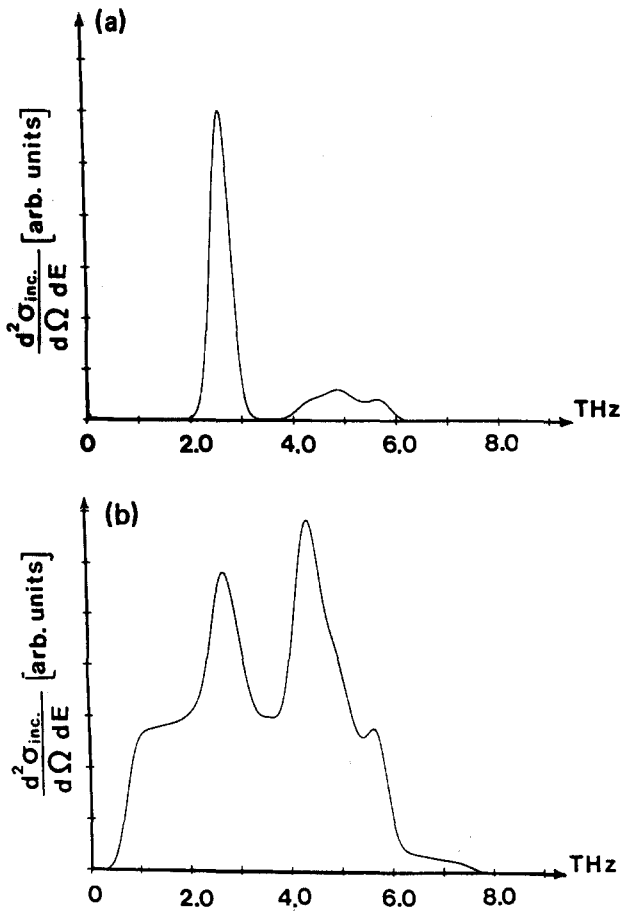

FIG. 12. Calculated inelastic neutron spectra of the S3 ethane monolayer phase assuming a Gaussian particle orientation distribution function: (a) **Q** perpendicular configuration; (b) **Q** parallel configuration. The spectra have been folded with a Gaussian resolution function (FWHM = 1.8 THz).

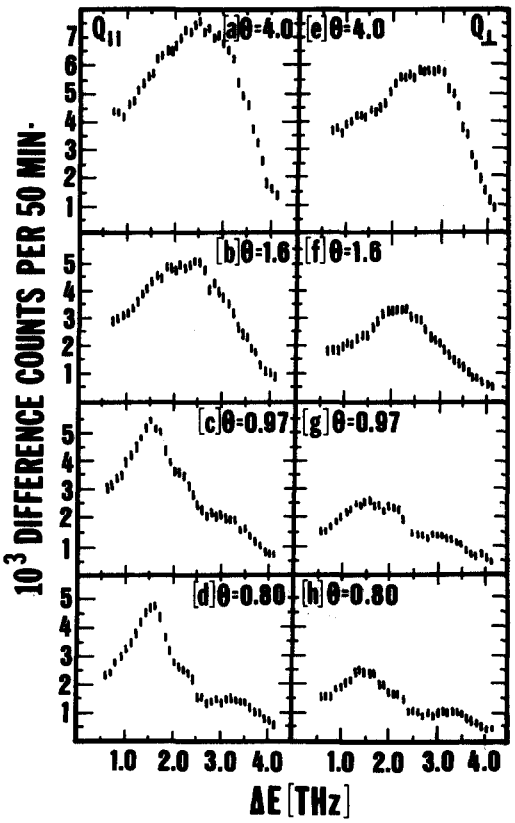

FIG. 13. Coverage (θ) dependence of the neutron energy-loss spectra from ethane adsorbed on Grafoil at 10 K. Spectra were taken at constant $Q = 4.0$ Å^{-1} in the parallel configuration [(a) through (d)] and in the perpendicular configuration [(e) through (h)]. Background scattering from the bare substrate has been subtracted from each spectrum.

Missouri Research Reactor Facility. The spectrometer was operated with a fixed incident energy of 33 meV and at a constant momentum transfer $\mathbf{Q} = |\mathbf{k}_f - \mathbf{k}_i|$ of either 2.2 or 4.0 Å^{-1}. Use of the Cu(200) reflection for both monochromator and analyzer crystals and 40′ collimation throughout gave an instrumental resolution (FWHM) of 0.4 THz (1.8 meV) in the energy transfer range $0.5 \leqslant \Delta E \leqslant 4.1$ THz. Different Grafoil sample cells were used for measurements in the **Q** parallel and perpendicular configurations. All spectra were obtained at a temperature of ~ 10 K by placing the cells in a closed-cycle helium refrigerator. They have been corrected for the energy dependence of the analyzer reflectivity.

Figure 13 shows the coverage dependence of the spectra at $Q = 4.0$ Å^{-1} in both the parallel and perpendicular configurations. Clearly, the S1 spectra at a coverage θ of 0.80 layers differ qualitatively from those of the S3 phase at 1.6 layers. It is also interesting to note that the spectra of the S2 phase[24] at 0.97 layers are qualitatively similar to the S1 spectra. Although it has been impossible to determine by elastic neutron diffraction the molecular orientations in the S2 phase, this similarity suggests that the molecules are lying with their C–C bond nearly parallel to the surface as in the S1 structure. At four layers, the spectra probably contain contributions from both bulk and film phases, since it is unlikely that ethane completely wets the graphite surface at this coverage.

The S3 spectra at 1.6 layers show little difference between the **Q** parallel and perpendicular configurations in contrast to the predictions in Fig. 12 for a Gaussian particle distribution. Similar calculations for the S1 phase also show a marked anisotropy between the two scattering directions which is not reflected in the observed spectra at 0.8 layers in Fig. 13. A possible explanation for these results is that most of the available surface area of the Grafoil substrate is contributed by smaller particles which have no preferred orientation. This interpretation is consistent with previous INS experiments with adsorbed Ar films[4] which indicated that at least 2/3 of the Grafoil surface to be oriented isotropically.

It seems appropriate, then, to compare the observed INS spectra with those calculated assuming an isotropic substrate. These spectra are shown at energy transfers up to 8 THz in Figs. 14(a) and 14(b) for the S3 and S1 phases, respectively. They have been calculated from Eq. (13) and then folded with the instrumental resolution function. In the case of the S1 phase, the coupling between the translational motion of the molecules normal to the surface and the lowest librational mode has been included as described in Sec. II. It can be seen from Fig. 14 that the calculated cross sections for the S3 and S1 phases differ greatly. To facilitate comparison with the observed spectra, we have replotted in Fig. 15 the calculated cross section for the S3 phase with that observed

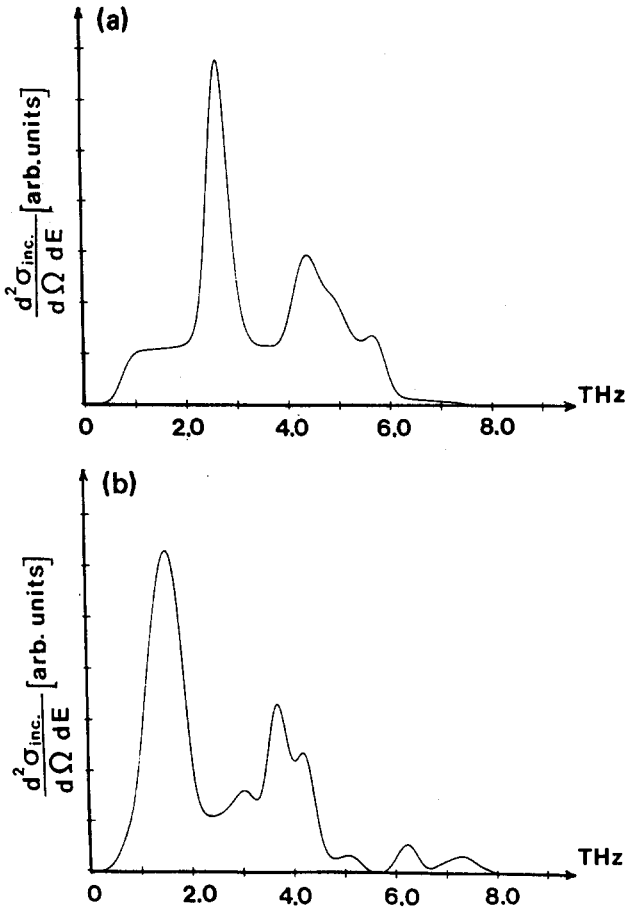

FIG. 14. Calculated inelastic neutron spectra of the (a) S3 and (b) S1 ethane monolayer phases assuming an isotropic powder substrate. The spectra have been folded with a Gaussian resolution function (FWHM = 1.8 THz).

at $Q = 4.0$ Å^{-1} (parallel configuration) at energy transfers up to 4.1 THz. Figure 16 contains the corresponding spectra for the S1 phase.

The dominant mode in the calculated spectrum for the S3 phase [Fig. 15(b)] is the molecular vibration normal to the surface (bouncing mode) at 2.6 THz. In this more densely packed phase in which the molecules stand on end, the librational modes occur at higher frequencies (see the dispersion curves in Fig. 5). The calculated peak for the bouncing mode is narrower and slightly higher in frequency than the observed band. The width observed may result from multiple scattering effects which become more severe as the coverage is increased.[41] It may also be related to a failure in the isotropic substrate assumption. The peak width is slightly greater in the parallel than in the perpendicular configuration [cf. Figs. 13(a) and 13(b)] in qualitative agreement with the Gaussian model calculations in Fig. 12.

There are two calculated spectra in Fig. 16(b) for the herringbone S1 phase. The dashed curve is the cross section calculated without the force constant coupling the bouncing motion of each molecule to its libration about a symmetry axis perpendicular to the C–C bond and parallel to the surface [see Fig. 1(b)]. It is dominated by a broadband at 2.8 THz contributed by both types of modes. Since there is a bouncing and librational mode for both molecules in the unit

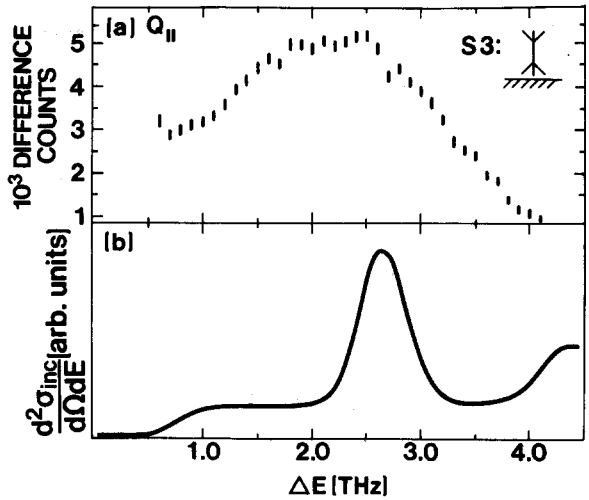

FIG. 15. Comparison of observed and calculated inelastic neutron spectra for the S3 ethane monolayer phase at 10 K. (a) Energy-loss spectrum observed at constant $Q = 4.0$ Å^{-1} with Q parallel to the Grafoil sheets [replotted from Fig. 13(b)]. (b) Calculated one-phonon cross section for the S3 phase [low-frequency portion of Fig. 14(a)].

cell, all four of the dashed branches in the dispersion relations of Fig. 9 contribute to this band. The agreement with the observed spectrum is poor in that its frequency is about a factor of 2 higher than that of the intense peak observed at 1.5 THz.

Rather than assume large errors in the force constants calculated for both the bouncing and librational modes, we investigated the effect of a coupling between them. Such a coupling appears plausible since the large distance of the CH_3 groups from the librational axis could result in a dependence of the librational restoring forces on the molecular height above the surface. The solid curve in Fig. 16(b) [see also Fig. 14(b)] represents the best fit to the observed spectrum which could be obtained by adjusting the strength of this coupling. The effect of the coupling is to split the band at

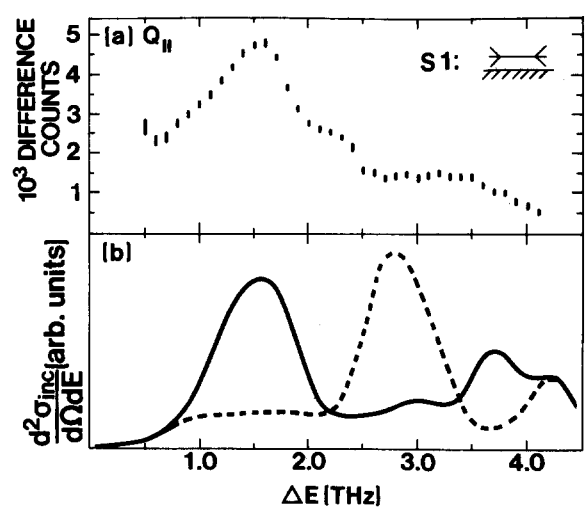

FIG. 16. Comparison of observed and calculated inelastic neutron spectra for the S1 ethane monolayer phase at 10 K. (a) Energy-loss spectrum observed at constant $Q = 4.0$ Å^{-1} with Q parallel to the Grafoil sheets [replotted from Fig. 13(d)]. (b) Calculated one-phonon cross sections for the S1 phase [low-frequency portion of Fig. 14(b)] as described in text.

2.8 THz into two peaks, the more intense of which reproduces well the band observed at 1.5 THz except for a shoulder seen at 2.3 THz. The weaker peak predicted at 3.7 THz is at a somewhat higher frequency than the band observed at 3.2 THz. As can be seen in Fig. 8, little dispersion is calculated for these coupled modes indicating their local character. On the other hand, the weak peak calculated at 3.0 THz corresponding to translational motion parallel to the surface is strongly dispersed. This mode together with the libration about the surface normal at 4.2 THz are unaffected by the coupling.

IV. SUMMARY AND CONCLUSIONS

The low-frequency vibrational modes in two crystalline monolayer phases of ethane adsorbed on the graphite (0001) surface have been studied theoretically and experimentally by inelastic neutron scattering. The sensitivity of INS to large-amplitude motion of H atoms has allowed investigation of low-frequency librational and translational modes of adsorbed ethane which are difficult to observe by other surface spectroscopies.

Our calculations with empirical atom–atom potentials reproduce the structure of the S1 and S3 monolayer phases reasonably well. The orientations predicted for the ethane molecule in the two phases agree with those deduced from elastic neutron diffraction experiments. The discrepancy between the calculated and observed lattice constants is less than 7%. This agreement motivated application of these potentials to calculations of the monolayer lattice dynamics including the phonon dispersion relations, the phonon density of states, and the phonon contribution to the heat capacities of the two phases. Contact with experiment was made through the one-phonon, incoherent neutron cross sections. The calculated spectra permit identification of the observed neutron energy-loss peaks and can account qualitatively for the difference in the neutron spectra of the two monolayer phases. Moreover, they suggest that an essential feature of the herringbone phase dynamics is a coupling of the lowest-frequency librational mode to the vibratory mode normal to the surface. A more quantitative comparison of calculated and observed INS spectra should probably await the development of empirical potentials which reproduce the observed monolayer structures more accurately. Better potentials would include the effects of intramolecular charge transfer and substrate mediated interactions.[42]

The INS spectra presented here provide some insight into the as yet unsolved structure of the S2 ethane phase which occurs in a narrow range of coverage near monolayer completion.[24] The similarity of the inelastic spectra of the S1 and S2 phases suggests that the latter may also have a herringbone-type structure in which the C–C bond of the molecule is nearly parallel to the surface. For example, it could be a striped phase in which commensurate herringbone regions are separated by narrow domain walls. It may be useful to reanalyze the neutron diffraction patterns of the S2 phase[8] using models of this type.

Finally, we would like to suggest the need for heat capacity experiments on the S1 and S3 ethane monolayer phases. These could provide an interesting check of the calculated phonon contribution to the specific heat shown in Figs. 7 and 11.

ACKNOWLEDGMENTS

We wish to thank R. Wang, H. Shechter, and H. R. Danner who participated in the experiments and J. M. Phillips for helpful discussions. D. G. Reichel and G. P. Alldredge assisted in the computations, and M. Assadollahbaik provided assistance in the figures. This work was partially supported by National Science Foundations Grant Nos. DMR-7905958 and DMR-8304366, a grant of the Petroleum Research Fund administered by the American Chemical Society, a Dow Chemical Company Grant of the Research Corporation, and a grant from the Danish Natural Science Foundation.

[1] See, for example, H. Taub, in *Vibrational Spectroscopies for Adsorbed Species*, edited by A. T. Bell and M. L. Hair, ACS Symp. Ser. No. 137 (American Chemical Society, Washington, D.C., 1980), p. 247.
[2] J. M. Szeftel, S. Lehwald, H. Ibach, T. S. Rahman, J. E. Black, and D. L. Mills, Phys. Rev. Lett. **51**, 268 (1983).
[3] K. D. Gibson and S. J. Sibener, Phys. Rev. Lett. **55**, 1514 (1985).
[4] H. Taub, K. Carneiro, J. K. Kjems, L. Passell, and J. P. McTague, Phys. Rev. B **16**, 4551 (1977).
[5] H. Taub, H. R. Danner, Y. P. Sharma, H. L. McMurry, and R. M. Brugger, Phys. Rev. Lett. **39**, 215 (1977); Surf. Sci. **76**, 50 (1978).
[6] B. H. Grier, L. Passell, J. Eckert, H. Patterson, D. Richter, and R. J. Rollefson, Phys. Rev. Lett. **53**, 814 (1984).
[7] B. F. Mason and B. R. Williams, Surf. Sci. **130**, L329 (1983).
[8] G. J. Trott, Ph. D. thesis, University of Missouri-Columbia, 1981 (unpublished).
[9] J. Suzanne, J. L. Seguin, H. Taub, and J. P. Biberian, Surf. Sci. **125**, 153 (1983).
[10] J. P. Coulomb, J. Suzanne, M. Bienfait, M. Matecki, A. Thomy, B. Croset, and C. Marti, J. Phys. (Paris) **41**, 1155 (1980).
[11] R. D. Diehl, M. F. Toney, and S. C. Fain, Jr., Phys. Rev. Lett. **43**, 1329 (1982).
[12] R. Wang, H. Taub, H. Shechter, R. Brener, J. Suzanne, and F. Y. Hansen, Phys. Rev. B **27**, 5864 (1983).
[13] J. Krim, J. Suzanne, H. Shechter, R. Wang, and H. Taub, Surf. Sci. **162**, 446 (1985); J. C. Newton, H. Taub, S.-K. Wang, and R. Wang, Bull. Am. Phys. Soc. **31**, 375 (1986).
[14] G. Bomchil, A. Hüller, R. Rayment, S. J. Roser, M. V. Smalley, R. K. Thomas, and J. W. White, Philos. Trans. R. Soc. London Ser. B **290**, 537 (1980).
[15] F. Y. Hansen, R. Wang, H. Taub, H. Shechter, D. G. Reichel, H. R. Danner, and G. P. Alldredge, Phys. Rev. Lett. **53**, 572 (1984).
[16] See, for example, K. Mirsky, in *Computing in Crystallography*, edited by H. Schenck (Delft University, Delft, 1978), p. 169.
[17] D. E. Williams, J. Chem. Phys. **45**, 3770 (1966).
[18] D. E. Williams, J. Chem. Phys. **47**, 4680 (1967).
[19] A. E. Kitaigorodskii, *Molecular Crystals* (Academic, New York, 1973).
[20] G. J. Trott, H. Taub, F. Y. Hansen, and H. R. Danner, Chem. Phys. Lett. **78**, 504 (1981).
[21] The H–H length scale $r_0 = 2.79$ Å for the Kitaigorodskii parameters is smaller than the $r_0 = 2.92$ Å used successfully for bulk methane [E. S. Severin and D. J. Tildesley, Mol. Phys. **41**, 1401 (1980)] and methane adsorbed on graphite [J. M. Phillips and M. D. Hammerbacher, Phys. Rev. B **29**, 5859 (1984)]. We are unaware of calculations on bulk or adsorbed methane with the Kitaigorodskii potentials.
[22] D. E. Williams and T. L. Starr, Comput. Chem. **1**, 173 (1977).
[23] F. Y. Hansen, G. P. Alldredge, L. W. Bruch, and H. Taub, J. Chem. Phys. **83**, 348 (1985).
[24] As discussed in Refs. 8 and 9, a third solid phase of ethane has been found

at low temperature in a narrow range of coverage near monolayer completion. This so-called S2 phase is believed to form a large-mesh superlattice ($10\times 2\sqrt{3}$) on the graphite basal plane (Ref. 9). Interpolation between the densities of the S1 and S3 phases suggests 12 molecules per unit cell. The molecular orientations have not been determined.

[25]We have assumed a cutoff length of 10 Å beyond which all three atom–atom potentials (C–C, C–H, and H–H) are taken to be zero. We believe this approximation is justified, since we are primarily concerned in these calculations with relative and not absolute interaction strengths.

[26]All molecules within the cluster are constrained to have the same height above the surface.

[27]M. Born and K. Huang, *Dynamical Theory of Crystal Lattices* (Oxford University, Oxford, 1968).

[28]K. A. Strong, AEC Report IN-1237, Idaho Nuclear Corp.

[29]H. Taub, H. J. Lauter, J. P. Biberian, and J. Suzanne (unpublished).

[30]F. Y. Hansen and H. Taub, Phys. Rev. B **19**, 6542 (1979).

[31]E. de Rouffignac, G. P. Alldredge, and F. W. de Wette, Phys. Rev. B **24**, 6050 (1981).

[32]F. W. DeWette, B. Firey, E. de Rouffignac, and G. P. Alldredge, Phys. Rev. B **28**, 4744 (1983).

[33]H. L. McMurry and F. Y. Hansen, J. Chem. Phys. **72**, 5540 (1980). This paper treats the lattice dynamics of Se and Te. The same method of expressing the intermolecular part of the potential energy function has also been applied to hexamethylenetetramine by these authors (unpublished).

[34]F. Y. Hansen, Comput. Phys. Commun. **14**, 193, 219 (1978).

[35]O. V. Kovalev, *Irreducible Representations of the Space Groups* (Gordon and Breach, New York, 1965).

[36]L. Radom and J. A. Pople, J. Am. Chem. Soc. **92**, 16, 4786 (1970).

[37]In the case of the S3 phase, several, but not all, of the off-diagonal elements can be shown to vanish at some wave vectors. However, the symmetry of the S1 phase is too low for such considerations to be useful.

[38]G. E. Bacon, *Thermal Neutron Diffraction*, 3rd ed. (Oxford University, Oxford, 1976).

[39]W. Marshall and S. W. Lovesey, *Theory of Thermal Neutron Scattering* (Oxford University, Oxford, 1971), pp. 86–87.

[40]Grafoil is the trademark of an expanded graphite product marketed by the Union Carbide Corp., Carbon Products Division, 270 Park Avenue, New York, NY 10017.

[41]According to Eq. (13) the intensity of the inelastic spectra should increase as Q^2 and their shape should be Q independent. We have obtained INS spectra from both the S1 and S3 phases at $Q = 2.2\ \text{Å}^{-1}$ (not shown). Although these spectra are weaker than those at $Q = 4.0\ \text{Å}^{-1}$, their intensity does not scale as Q^2. Also, the $Q = 2.2\ \text{Å}^{-1}$ spectra differ somewhat in shape; for example, a greater width is observed for the main peak in the S3 spectrum (perpendicular configuration). These Q-dependent features of the spectra may be caused by multiple scattering effects.

[42]A comparison of the observed S1 and S3 ethane monolayer structures on graphite with calculations which include electrostatic and substrate mediated interactions is in progress [F. Y. Hansen and H. Taub (unpublished)].